

# Ultrahigh energy storage density in epitaxial AlN/ScN superlattices

Zhijun Jiang,<sup>1,2,3</sup> Bin Xu,<sup>4,\*</sup> Hongjun Xiang,<sup>1,5,6,†</sup> and L. Bellaiche<sup>2</sup>

<sup>1</sup>Key Laboratory of Computational Physical Sciences (Ministry of Education),  
State Key Laboratory of Surface Physics, and Department of Physics, Fudan University, Shanghai 200433, China

<sup>2</sup>Physics Department and Institute for Nanoscience and Engineering,  
University of Arkansas, Fayetteville, Arkansas 72701, USA

<sup>3</sup>MOE Key Laboratory for Nonequilibrium Synthesis and Modulation of Condensed Matter,  
School of Physics, Xi'an Jiaotong University, Xi'an 710049, China

<sup>4</sup>Jiangsu Key Laboratory of Thin Films, School of Physical Science and Technology, Soochow University, Suzhou 215006, China

<sup>5</sup>Collaborative Innovation Center of Advanced Microstructures, Nanjing 210093, China

<sup>6</sup>Shanghai Qi Zhi Institute, Shanghai 200232, China

Dielectric and antiferroelectric materials are particularly promising for high-power energy-storage applications. However, relatively low energy density greatly hinders their usage in storage technologies. Here, we report first-principles-based calculations predicting that epitaxial and initially non-polar AlN/ScN superlattices can achieve an ultrahigh energy density of up to 200 J/cm<sup>3</sup>, accompanied by an ideal efficiency of 100%. We also show that high energy density requires the system being neither too close nor too far from a ferroelectric phase transition under zero electric field. A phenomenological model is further proposed to rationalize such striking features.

Electrostatic capacitors that are based on dielectric or antiferroelectric materials are promising energy storage components in various electronic applications because of their higher power density, faster charging/discharging rates, and better stability when compared with supercapacitors and batteries [1–16]. However, their relatively low energy density is the main bottleneck towards energy-storage applications, while intensive efforts have been devoted to find novel compounds with improved storage properties. In general, the recoverable energy density ( $U_{\text{rec}}$ ) is determined by the work done by the electric field during discharging,  $U_{\text{rec}} = \int_{P_r}^{P_{\text{max}}} E dP$ , where  $P_{\text{max}}$  and  $P_r$  are the maximum and remnant polarization, respectively. To achieve high energy density, it is usually required to have high  $P_{\text{max}}$ , low  $P_r$ , and high breakdown strength [5–10]. The efficiency is defined as  $\eta = [U_{\text{rec}}/(U_{\text{rec}} + U_{\text{loss}})] \times 100\%$ , where  $U_{\text{loss}}$  is the energy loss density. Therefore, a linear dielectric material has an energy density ( $U$ ) of  $U = \frac{1}{2}\epsilon_0\epsilon_r E^2$ , where  $\epsilon_0$  is the vacuum permittivity,  $\epsilon_r$  is the relative permittivity, and  $E$  is the electric field. Obviously, high values of permittivity  $\epsilon_r$  and breakdown strength  $E_{\text{break}}$  lead to large energy density [17–19]. On the other hand, nonlinear dielectrics – usually including ferroelectrics, antiferroelectric, and relaxors – have either low energy density (in ferroelectrics) or dissipative energy losses that can reduce efficiency (in antiferroelectrics and relaxors). For instance, the energy density is low for a ferroelectric material, due to large remnant polarization [19].

To maximize both energy density and efficiency, one can in fact imagine a nonlinear type dielectric material that can combine the advantages of a ferroelectric and a linear dielectric, i.e., possessing large polarization under high field, and being nonpolar under zero field as well as reversible. This would require the nonlinear dielectrics to have large  $\epsilon_r$  and high  $E_{\text{break}}$  [11–16]. A promising candidate is the III-V semiconductor-based systems made by mixing AlN and ScN to form  $\text{Al}_{1-x}\text{Sc}_x\text{N}$  solid solutions or AlN/ScN superlattices,

that have been attracting much attention due to their potential for high piezoelectric and electro-optic responses [20–29]. Note that a recent experiment observed a ferroelectric switching in  $\text{Al}_{1-x}\text{Sc}_x\text{N}$  films, with a remnant polarization reaching a very large value – in excess of 1.0 C/m<sup>2</sup> [25] – which contrasts with the case of pure AlN that is of wurtzite-type structure [30, 31] and is polar but not ferroelectric. Note that for larger Sc compositions (above 43%),  $\text{Al}_{1-x}\text{Sc}_x\text{N}$  can be non-polar [20, 21, 25].

The aim of this Letter is to demonstrate and explain why very promising energy-storage can be achieved in (Al,Sc)N systems being initially in a non-polar phase but at close proximity with a ferroelectric state that is easy to reach under electric fields.

Here, first-principles calculations are performed on (001) epitaxial  $1 \times 1$  AlN/ScN superlattices within the local density approximation (LDA) to the density functional theory (DFT), as implemented in the ABINIT package [32]. The epitaxial strain is defined as  $\eta_{\text{in}} = (a - a_{\text{eq}})/a_{\text{eq}}$ , where  $a_{\text{eq}}$  is the in-plane lattice constant corresponding to the equilibrium  $P\bar{6}m2$  phase of bulk  $1 \times 1$  AlN/ScN superlattices [27]. A  $6 \times 6 \times 4$   $k$ -point mesh and a plane-wave kinetic energy cutoff of 50 Hartree and of 60 Hartree are employed for structural relaxation. The higher value of 60 Hartree is used to minimize the Pulay error in the stress. A  $dc$  electric field,  $E$ , is applied along the [001] direction ( $c$ -axis) by adopting the method developed in Refs. [33–36]. For each field-induced structure, the electrical polarization,  $P$ , along the  $c$ -axis is computed from the Berry phase method [37, 38] and  $P$ - $E$  curves are then obtained. Note that, for each chosen strain and applied  $dc$  electric field, the in-plane lattice vectors are kept fixed during the simulations while the out-of-plane lattice vector and atomic positions are fully relaxed, until the force on each atom is smaller than  $10^{-6}$  Hartree/Bohr – in order to simulate *epitaxial* films under electric field.

Due to Landauer’s paradox, the theoretical electric field is

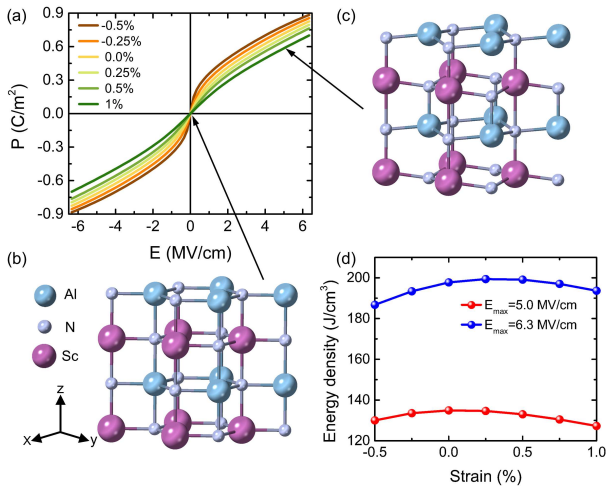


FIG. 1. (a)  $P$ - $E$  hysteresis curves with different epitaxial strains with the ground state being a hexagonal-derived structure in  $1 \times 1$  AlN/ScN superlattices. Crystal structures of 1% tensile strain under electric fields of (b) 0 MV/cm and (c) 5 MV/cm, respectively, in  $1 \times 1$  AlN/ScN superlattices. (d) Energy density versus misfit strain for two different ending electric fields of 5.0 MV/cm and 6.3 MV/cm.

typically larger compared with measurement [9, 39–42], and the electric fields considered in this Letter have been rescaled by a factor of 1/3, in order that the  $P$ - $E$  loop of the  $1 \times 1$  AlN/ScN system under a  $-3\%$  strain matches the experimental one corresponding to a  $\text{Al}_{0.57}\text{Sc}_{0.43}\text{N}$  film [25] – as demonstrated in Fig. S1 of the Supplemental Material (SM) [43]. Note that such rescaling of computational electric fields is material-dependent but not phase-dependent for a given material [39]. For instance, Ref. [39] demonstrated that a rescaling of the electric field is able to reproduce very well the electric field-versus-temperature phase diagram of the complex  $\text{Pb}(\text{Mg},\text{Nb})\text{O}_3$  system, with this phase diagram involving different phases (e.g., relaxor paraelectric *versus* ferroelectric) and even different orders (first *versus* second) of the phase transitions. Regarding the magnitude of the (renormalized) fields to be considered here, it is first worthwhile to indicate that a recent experiment reported a feasible electric field as high as  $\simeq 5$  MV/cm in  $\text{Al}_{1-x}\text{Sc}_x\text{N}$  films [25]. Moreover, one can also estimate the intrinsic breakdown field of such systems empirically, which depends on the band gap [47]. Our predicted gap of 3.1 eV after correction (to account for the typical underestimation of LDA) of the  $1 \times 1$  AlN/ScN superlattice ground state [27] yields an intrinsic breakdown field,  $E_{\text{break}}$ , of 6.3 MV/cm, which will be the maximum fields considered here. Note that the estimated breakdown field is reasonable since (1) Yazawa *et al.* reported the highest applied electric field ( $\sim 6$  MV/cm) in epitaxial  $\text{Al}_{0.7}\text{Sc}_{0.3}\text{N}$  film [28]; and (2) Yasuoka *et al.* also reported very large coercive fields of the order of 4-7 MV/cm and maximum applicable electric fields of the order 5-10 MV/cm in  $\text{Al}_{1-x}\text{Sc}_x\text{N}$  films [29].

For the  $1 \times 1$  AlN/ScN superlattices under different epitaxial strains, previous studies have predicted the existence of

different phases [26, 27], including a wurtzite-derived structure (polar  $P3m1$  space group with a polarization along the  $c$ -axis) and a hexagonal-derived structure (non-polar  $P6m2$  space group). They are related to each other by a continuous change in the internal parameter ( $u$ ) and the axial ratio ( $c/a$ ) [27]. Figure 1(a) shows the  $P$ - $E$  curves for strain values larger than  $-0.5\%$  (from compressive to tensile), with the hexagonal-derived structure as ground state [see Fig. 1(b) for such structure at 1% strain under zero field]. The structure associated with the electric field of 5 MV/cm is polar and close to the wurtzite-derived structure [see Fig. 1(c)].

When the strain is between  $-5\%$  and  $-1\%$  (as shown in Fig. S1(b) of the SM [43]) the  $P$ - $E$  loops show typical single hysteresis of ferroelectrics with switching of polarization between the two degenerate wurtzite-derived structures, and the magnitudes of the critical fields depend very strongly on strain. Similar strong dependency was also observed in  $\text{Al}_{1-x}\text{Sc}_x\text{N}$  solid solutions with respect to the Sc composition [25]; therefore, it suggests that varying composition in the solid solution or changing the strain for a fixed alloy or superlattice may involve similar physics. Due to the strong strain dependency, the hysteresis rapidly shrinks with reduced compressive strain, and completely vanishes beyond  $-0.5\%$  strain, as depicted in Fig. 1(a). In this range of strains, the ground state becomes the non-polar  $P6m2$  hexagonal-derived phase. More interestingly, the  $P$ - $E$  curve is very nonlinear at small compressive strain (e.g.,  $-0.5\%$ ) – starting with large dielectric susceptibility at small field and saturating at elevated field – while it becomes more linear as the strain increases (e.g.,  $1\%$ ). And the transition to the polar wurtzite-type phase is predicted to be continuous and fully reversible upon increasing and decreasing electric fields.

Let us now check the energy storage properties for the  $1 \times 1$  AlN/ScN superlattices for misfit strains varying between  $-0.5\%$  to  $+1\%$ . The first feature to realize is that the energy efficiency is automatically 100% because the charging and discharging processes are completely reversible, as revealed by the continuous  $P$ - $E$  curves of Fig. 1(a). The energy density is depicted in Fig. 1(d) for epitaxial strain ranging between  $-0.5\%$  and  $+1\%$ , with the maximal applied electric field being 5 MV/cm that has been realized experimentally [25] in this type of nitride semiconductors, and 6.3 MV/cm estimated as the intrinsic breakdown field. It is striking that the energy density reaches (slightly strain-dependent) values varying between 127 and 135  $\text{J}/\text{cm}^3$  and between 187 and 200  $\text{J}/\text{cm}^3$  when using 5 MV/cm and 6.3 MV/cm for the largest applied field, respectively. All these energy densities and efficiencies are thus predicted to be giant, since they are much larger than those measured in lead-based and lead-free dielectric thin films [6, 12, 14, 15, 48–51], such as  $(\text{Bi}_{0.5}\text{Na}_{0.5})_{0.9118}\text{La}_{0.02}\text{Ba}_{0.0582}(\text{Ti}_{0.97}\text{Zr}_{0.03})\text{O}_3$  (BNLBTZ) epitaxial relaxor (154  $\text{J}/\text{cm}^3$  and 97% for a maximum applied field,  $E_{\text{max}} = 3.5$  MV/cm) [6],  $\text{BiFeO}_3$ - $\text{BaTiO}_3$ - $\text{SrTiO}_3$  solid solutions (112  $\text{J}/\text{cm}^3$  and 80% for  $E_{\text{max}} = 4.9$  MV/cm) [12],  $\text{Pb}_{0.88}\text{Ca}_{0.12}\text{ZrO}_3$  (91.3  $\text{J}/\text{cm}^3$  and 85.3% for  $E_{\text{max}} = 5$  MV/cm) [14], and ion-bombarded relaxor ferroelectric

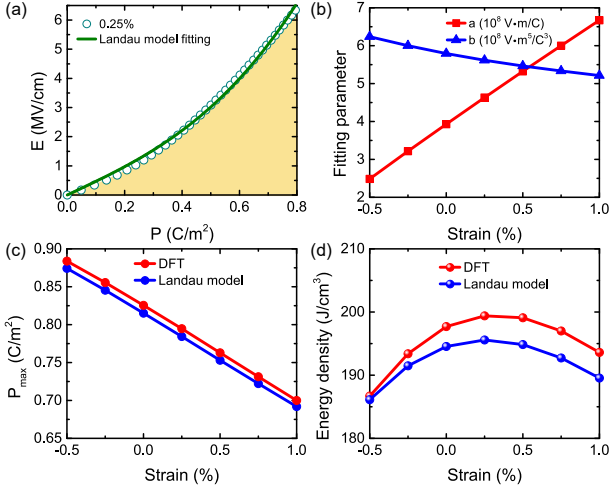


FIG. 2. (a) Electric field versus polarization for strains at 0.25% (the solid green line represents the fit of the DFT results by the Landau model), with the yellow area showing the energy density. (b) Evolution with strain of fitting parameters  $a$  and  $b$  (see text). Strain-dependence of (c)  $P_{\max}$  and (d) energy density results obtained from DFT and Landau model. These data correspond to a maximal applied electric field of  $E_{\text{break}} = 6.3$  MV/cm.

0.68Pb(Mg<sub>1/3</sub>Nb<sub>2/3</sub>)O<sub>3</sub>-0.32PbTiO<sub>3</sub> (PMN-PT) films (133 J/cm<sup>3</sup> and 75% for  $E_{\max} = 5.9$  MV/cm) [15]. The 100% efficiency and the giant energy densities suggest that the 1×1 AlN/ScN superlattices are highly promising for energy-storage applications.

To understand these results, let us recall that, a nonlinear dielectric with no energy dissipation has an energy density  $U$  has the following form:

$$U = \int_0^{P_{\max}} E dP, \quad (1)$$

where  $P_{\max}$  is the maximum polarization, exhibited at the highest applied field,  $E_{\max}$ . Figure 2(a) displays the (positive) electric field applied along the [001] pseudo-cubic direction as a function of polarization for one particular misfit strain at 0.25%. The area shown in yellow of Fig. 2(a) is the energy density.

The energy density in Fig. 1(d) can be understood based on a simple Landau-type free energy that describes the behavior of a nonlinear dielectric:

$$F = \frac{1}{2}aP^2 + \frac{1}{4}bP^4 - EP, \quad (2)$$

where  $a$  and  $b$  are coefficients of the quadratic and quartic terms, respectively, and they are positively defined for a paraelectric or non-polar phase.

Noting that at equilibrium condition, we have  $\frac{\partial F}{\partial P} = 0$ , which leads to

$$E = aP + bP^3. \quad (3)$$

Thus, the polarization is zero without the application of an electric field. Consequently, the energy density can be written in the simple following form:

$$U = \int_0^{P_{\max}} (aP + bP^3) dP = \frac{1}{2}aP_{\max}^2 + \frac{1}{4}bP_{\max}^4. \quad (4)$$

As shown in Fig. 2(a), the electric field versus polarization ( $E$ - $P$ ) data for strains at 0.25% can be very well fitted by Eq. (3). In fact, Eq. (3) fits remarkably well the DFT  $E$ - $P$  data for all the considered strain ranging between  $-0.5\%$  and  $+1\%$  (see Fig. S3 of the SM [43]). Figure 2(b) shows the fitting parameters  $a$  and  $b$  as a function of epitaxial strain ranging between  $-0.5\%$  and  $+1\%$ , for electric fields up to the intrinsic breakdown field  $E_{\max} = E_{\text{break}} = 6.3$  MV/cm. Interestingly, Fig. 2(b) reveals that the fitting parameter  $a$  linearly increases when the strain increases from  $-0.5\%$  to  $+1\%$  ( $a$  varies from  $2.5 \times 10^8$  V·m/C to  $6.7 \times 10^8$  V·m/C). In contrast, the  $b$  parameter linearly decreases with strain, with the change of  $b$  being much smaller in percentage than  $a$  and taking values ranging between  $6.2 \times 10^8$  V·m<sup>5</sup>/C<sup>3</sup> and  $5.2 \times 10^8$  V·m<sup>5</sup>/C<sup>3</sup>. Note that the  $a$  parameter of the Landau expansion is negative in our phenomenology model when the ground state of the superlattice is ferroelectric (see Fig. S4 of the SM [43]).

Figure 2(c) displays the value of the polarization,  $P_{\max}$ , for  $E_{\max} = 6.3$  MV/cm, as a function of strain both from DFT calculations and the Landau model using the DFT-fitted  $a$  and  $b$  in Eq. (3). One can first clearly see that, for any of these strains, the DFT and Landau model provide nearly identical results. According to Fig. 2(c),  $P_{\max}$  is larger than  $0.7$  C/m<sup>2</sup> for any considered strain ranging between  $-0.5\%$  and  $+1\%$ , which reflects that the structure at such high field is wurtzite-like. Note that, for  $E_{\max} = E_{\text{break}}$ ,  $P_{\max}$  linearly decreases with strain from  $0.88$  to  $0.70$  C/m<sup>2</sup>, which can be simply understood by the fact that increasing strains towards and within the tensile regime is known to reduce the out-of-plane polarization in ferroelectric systems [26, 52, 53].

To understand the results in Fig. 1(d), we use Eq. (4) to obtain the energy density for different strains at  $E_{\max} = 6.3$  MV/cm. Figure 2(d) shows that the Landau model agrees rather well with the DFT-obtained energy density, with an excellent agreement at small strain and a slightly increasing discrepancy at larger strains (less than 2% at 1.0% strain), implying the validity of the Landau model. Equation (4) tells us that the energy density is the sum of two terms – that are  $\frac{1}{2}aP_{\max}^2$  and  $\frac{1}{4}bP_{\max}^4$ . The first contribution depends on the product of the  $a$  parameter and  $P_{\max}^2$ , and is numerically found to increase when the strain is enhanced between  $-0.5\%$  and  $+1\%$  (see Fig. S5 of the SM [43]). The second contribution is the product between the  $b$  parameter and  $P_{\max}^4$ , and decreases with strain since  $b$  slightly decreases when changing the strain from  $-0.5\%$  to  $+1\%$  while  $P_{\max}$  is reduced with strain, as a consequence of the aforementioned coupling between out-of-plane polarization and in-plane strains [see Figs. 2(b) and 2(c)]. Practically, the contribution of  $\frac{1}{2}aP_{\max}^2$  (respectively, of  $\frac{1}{4}bP_{\max}^4$ ) to the total energy density is 51% (respectively,

49%), 73% (respectively, 27%), and 84% (respectively, 16%) for strains at  $-0.5\%$ ,  $0.25\%$ , and  $1\%$ , respectively. Note also that the strain dependency of  $\frac{1}{2}aP_{\max}^2$  and  $\frac{1}{4}bP_{\max}^4$ , along with the dependency of  $P_{\max}$  on  $E_{\max}$  [see Fig. 1(a)], leads to a maximum value of the total energy density  $U$  occurring at a specific strain for a given  $E_{\max}$ , while different  $E_{\max}$  can further quantitatively modulate the performance. For instance, such maximum occurs at  $0\%$  and  $0.25\%$  misfit strain when the largest applied field is  $5\text{ MV/cm}$  and  $6.3\text{ MV/cm}$ , respectively [see Fig. 1(d)].

As evidenced above, we numerically found that the energy density at its maximum value, for our selected  $E_{\max}$  of  $6.3\text{ MV/cm}$ , mostly (i.e., at  $73\%$ ) depends on the  $a$  parameter and  $P_{\max}$  via  $\frac{1}{2}aP_{\max}^2$ . Let us thus fix  $b$  as a constant and vary the  $a$  parameter for the case of  $E_{\max} = 6.3\text{ MV/cm}$ , and compute the resulting  $P_{\max}$  and energy density using Eqs. (3) and (4). The results are shown in Fig. S6 of the SM [43]), which reveal that the energy density varies non-monotonically with the  $a$  parameter at a selected strain of  $0.25\%$ , presenting a maximum,  $U_{\max, b\text{-fixed}}$ , for an intermediate  $a$  value. Note that small  $a$  gives smaller density than  $U_{\max, b\text{-fixed}}$  because  $\frac{1}{2}aP_{\max}^2$  is reduced via the  $a$  parameter; while larger  $a$  also provides an energy density being smaller than  $U_{\max, b\text{-fixed}}$  because now  $P_{\max}$  is weakened in  $\frac{1}{2}aP_{\max}^2$ . These facts automatically imply that there is a trade-off to have large energy density: the system should not be too close (i.e., should not have a very small  $a$ ) but also not be too far (i.e., should not possess a too large  $a$ ) from a ferroelectric phase transition.

In summary, we have performed first-principles calculations to investigate the energy-storage properties and out-of-plane strains in epitaxial  $1\times 1\text{ AlN/ScN}$  superlattices. We find that these systems exhibit very high energy-densities up to  $200\text{ J/cm}^3$  and an ideal  $100\%$  efficiency, as well as ultra-high strain levels of about  $10\%$  (see Fig. S2 of the SM [43]). Note that InN can be used as a substrate to get  $0.3\%$  of strain [27] to achieve the predicted performance, which is promising for energy storage in our proposed system. Such unusual and promising features originate from high values of the electric field that can be applied in these systems, and in particular from a nonlinear electric-field-induced strong polarizability of the non-polar hexagonal-like polymorph. A simple Landau model is developed to analyze and understand these results, which also suggests that (Al,Sc)N disordered solid solutions should also possess these “wunderbar” properties for compositions lying in the non-polar regime near but not too close to the border with the wurtzite-like structure. The proposed new concept of using nonlinear and non-polar systems close to a ferroelectric state as an energy storage material is general and we expect that other materials with similar characteristics are also good candidates for energy storage.

This work is supported by the National Natural Science Foundation of China (Grants No. 11804138, No. 11825403, and No. 11991061), Shandong Provincial Natural Science Foundation (Grant No. ZR2019QA008), China Postdoctoral Science Foundation (Grants No. 2020T130120 and No. 2018M641905), the Qing Nian Ba Jian Program, Postdoc-

toral International Exchange Program of Academic Exchange Project, Fudan University Super Postdoctoral Program, and Shanghai Post-doctoral Excellence Program. B. X. acknowledges financial support from National Natural Science Foundation of China (Grant No. 12074277), the startup fund from Soochow University and support from Priority Academic Program Development (PAPD) of Jiangsu Higher Education Institutions. L. B. acknowledges the DARPA grant HR0011-15-2-0038 (MATRIX program).

\* [binxu19@suda.edu.cn](mailto:binxu19@suda.edu.cn)

† [hxiang@fudan.edu.cn](mailto:hxiang@fudan.edu.cn)

- [1] B. Chu, X. Zhou, K. Ren, B. Neese, M. Lin, Q. Wang, F. Bauer, and Q. M. Zhang, *Science* **313**, 334 (2006).
- [2] X. Hao, *J. Adv. Dielectr.* **3**, 1330001 (2013).
- [3] S. Patel, A. Chauhan, and R. Vaish, *Mater. Res. Express* **1**, 045502 (2014).
- [4] Q. Li *et al.*, *Nature* **523**, 576 (2015).
- [5] A. Chauhan, S. Patel, R. Vaish, and C. R. Bowen, *Materials* **8**, 8009 (2015).
- [6] B. Peng *et al.*, *Adv. Electron. Mater.* **1**, 1500052 (2015).
- [7] Prateek, V. K. Thakur, and R. K. Gupta, *Chem. Rev.* **116**, 4260 (2016).
- [8] Z. Yao, Z. Song, H. Hao, Z. Yu, M. Cao, S. Zhang, M. T. Lanagan, and H. Liu, *Adv. Mater.* **29**, 1601727 (2017).
- [9] B. Xu, J. Íñiguez, and L. Bellaiche, *Nat. Commun.* **8**, 15682 (2017).
- [10] H. Huang and J. F. Scott, *Ferroelectric Materials for Energy Applications* (Wiley, Weinheim, 2018).
- [11] L. Yang, X. Kong, F. Li, H. Hao, Z. Cheng, H. Liu, J.-F. Li, and S. Zhang, *Prog. Mater. Sci.* **102**, 72 (2019).
- [12] H. Pan *et al.*, *Science* **365**, 578 (2019).
- [13] K. Zou, Y. Dan, H. Xu, Q. Zhang, Y. Lu, H. Huang, and Y. He, *Mater. Res. Bull.* **113**, 190 (2019).
- [14] Y. Z. Li, J. L. Lin, Y. Bai, Y. X. Li, Z. D. Zhang, and Z. J. Wang, *ACS Nano* **14**, 6857 (2020).
- [15] J. Kim, S. Saremi, M. Acharya, G. Velarde, E. Parsonnet, P. Donahue, A. Qualls, D. Garcia, and L. W. Martin, *Science* **369**, 81(2020).
- [16] M. Peddigari, H. Palneedi, G.-T. Hwang, and J. Ryu, *J. Korean Ceram. Soc.* **56**, 1 (2019).
- [17] H. Y. Zhou, X. N. Zhu, G. R. Ren, and X. M. Chen, *J. Alloys Compd.* **688**, 687 (2016).
- [18] H. Y. Zhou, X. Q. Liu, X. L. Zhu, and X. M. Chen, *J. Am. Ceram. Soc.* **101**, 1999 (2018).
- [19] Q. Li, F. Z. Yao, Y. Liu, G. Zhang, H. Wang, and Q. Wang, *Annu. Rev. Mater. Sci.* **48**, 219 (2018).
- [20] M. Akiyama, T. Kamohara, K. Kano, A. Teshigahara, Y. Takeuchi, and N. Kawahara, *Adv. Mater.* **21**, 593 (2009).
- [21] M. Akiyama, K. Kano, and A. Teshigahara, *Appl. Phys. Lett.* **95**, 162107 (2009).
- [22] F. Tasnádi, B. Alling, C. Höglund, G. Wingqvist, J. Birch, L. Hultman, and I. A. Abrikosov, *Phys. Rev. Lett.* **104**, 137601 (2010).
- [23] S. Zhang, D. Holec, W. Y. Fu, C. J. Humphreys, and M. A. Moram, *J. Appl. Phys.* **114**, 133510 (2013).
- [24] P. Daoust, P. Desjardins, R. A. Masut, V. Gosselin, and M. Côté, *Phys. Rev. Mater.* **1**, 055402 (2017).
- [25] S. Fichtner, N. Wolff, F. Lofink, L. Kienle, and B. Wagner, *J.*

- Appl. Phys. **125**, 114103 (2019).
- [26] M. Noor-A-Alam, O. Z. Olszewski, and M. Nolan, ACS Appl. Mater. Interfaces **11**, 20482 (2019).
- [27] Z. Jiang, C. Paillard, D. Vanderbilt, H. Xiang, and L. Bellaiche, Phys. Rev. Lett. **123**, 096801 (2019).
- [28] K. Yazawa, D. Drury, A. Zakutayev, and G. L. Brennecke, arXiv:2101.06612.
- [29] S. Yasuoka, T. Shimizu, A. Tateyama, M. Uehara, H. Yamada, M. Akiyama, Y. Hiranaga, Y. Cho, and H. Funakubo, J. Appl. Phys. **128**, 114103 (2020).
- [30] A. F. Wright and J. S. Nelson, Phys. Rev. B **51**, 7866 (1995).
- [31] C. Bungaro, K. Rapcewicz, and J. Bernholc, Phys. Rev. B **61**, 6720 (2000).
- [32] X. Gonze, J.-M. Beuken, R. Caracas, F. Detraux, M. Fuchs, G.-M. Rignanese, L. Sindic, M. Verstraete, G. Zerah, F. Jollet, M. Torrent, A. Roy, M. Mikami, Ph. Ghosez, J.-Y. Raty, and D. C. Allan, Comput. Mater. Sci. **25**, 478 (2002).
- [33] R. W. Nunes and D. Vanderbilt, Phys. Rev. Lett. **73**, 712 (1994).
- [34] R. W. Nunes and X. Gonze, Phys. Rev. B **63**, 155107 (2001).
- [35] I. Souza, J. Íñiguez, and D. Vanderbilt, Phys. Rev. Lett. **89**, 117602 (2002).
- [36] J. W. Zwanziger, J. Galbraith, Y. Kipouros, M. Torrent, M. Giantomassi, X. Gonze, Comput. Mater. Sci. **58**, 113 (2012).
- [37] R. D. King-Smith and D. Vanderbilt, Phys. Rev. B **47**, 1651 (1993).
- [38] R. Resta, Rev. Mod. Phys. **66**, 899 (1994).
- [39] Z. Jiang, Y. Nahas, S. Prokhorenko, S. Prosandeev, D. Wang, J. Íñiguez, and L. Bellaiche, Phys. Rev. B **97**, 104110 (2018).
- [40] J. Lu, G. Chen, W. Luo, J. Íñiguez, L. Bellaiche, and H. Xiang, Phys. Rev. Lett. **122**, 227601 (2019).
- [41] L. Chen, C. Xu, H. Tian, H. Xiang, J. Íñiguez, Y. Yang, and L. Bellaiche, Phys. Rev. Lett. **122**, 247701 (2019).
- [42] Z. Jiang, C. Paillard, H. Xiang, and L. Bellaiche, Phys. Rev. Lett. **125**, 017401 (2020).
- [43] See Supplemental Material at ... for more details about (i) the renormalization factor of the theoretical fields; (ii) out-of-plane strain versus electric field; and (iii) using a simple Landau model to understand the energy storage results in  $1 \times 1$  AlN/ScN superlattices, which includes Refs. [44-46].
- [44] S.-E. Park and T. R. ShROUT, J. Appl. Phys. **82**, 1804 (1997).
- [45] B. Jaffe, W. R. Cook, and H. Jaffe, *Piezoelectric Ceramics* (Academic Press, London, 1971).
- [46] C. A. Randall, A. Kelnberger, G. Y. Yang, R. E. Eitel, and T. R. ShROUT, J. Electroceram. **14**, 177 (2005).
- [47] L.-M. Wang, Relationship between Intrinsic Breakdown Field and Bandgap of Materials. *25th International Conference on Microelectronics* (Belgrade, 2006).
- [48] M. H. Park, H. J. Kim, Y. J. Kim, T. Moon, K. D. Kim, and C. S. Hwang, Adv. Energy Mater. **4**, 1400610 (2014).
- [49] B. Ma, Z. Hu, R. E. Koritala, T. H. Lee, S. E. Dorris, and U. Balachandran, J. Mater. Sci. Mater. Electron. **26**, 9279 (2015).
- [50] Z. Sun, C. Ma, M. Liu, J. Cui, L. Lu, J. Lu, X. Lou, L. Jin, H. Wang, and C.-L. Jia, Adv. Mater. **29**, 1604427 (2017).
- [51] H. Pan *et al.*, Nat. Commun. **9**, 1813 (2018).
- [52] Y. Yang, W. Ren, M. Stengel, X. H. Yan, and L. Bellaiche, Phys. Rev. Lett. **109**, 057602 (2012).
- [53] L. Chen, Y. Yang, Z. Gui, D. Sando, M. Bibes, X. K. Meng, and L. Bellaiche, Phys. Rev. Lett. **115**, 267602 (2015).